NOVA SCHOOL OF SCIENCE & TECHNOLOGY

MATERIALS SCIENCE DEPARTMENT

FREDERICO VICTORINO GALVÃO VIDEIRA

Bachelor in Materials Engineering

LASER PROCESSING OF CoCrFeMnNi HIGH ENTROPY ALLOYS

Supervisor: Professor João Pedro Oliveira, DCM

Co-Supervisor: Jiajia Shen

MASTER IN MATERIALS ENGINEERING

Universidade NOVA de Lisboa

September, 2022

Laser Processing of CoCrFeMnNi High Entropy Alloys

To my family

ACKNOWLEDGEMENTS

First, I would like to thank my supervisor and professor João Pedro Oliveira for giving me the opportunity to study an interesting and challenging theme, for all his teachings, and for all the help he gave me. Also, a very special word to Jiajia Shen, for her role as my co-supervisor in this thesis. I couldn't have done it without her, thank you for all the unconditional patience and all the help in both practical and written work.

Regarding my second home for the past 5 years, NOVA SST was a great experience where I always felt good. A lot of friends were made and a lot of knowledge was acquired. A word for the Materials' department that provided all its knowledge to make us good professionals for the future, but also for looking out to its students all times.

Thanks to my Family for all the unconditional support during the past 5 years of my life which I can say that, even with a change from Environmental to Materials' engineering, went pretty well. In my opinion, a very important acknowledgement is that Family is our foundation and without it, things can get rough.

Finally, my girlfriend Maria do Carmo and all my closest friends that establish a very important pillar in my life with whom I shared a lot of important moments during this time. Five rewarding years of study, having fun, travelling, and getting my Master's degree.

Thank you all!

"Perseverance is not a long race; it is many short races one after the other."

Walter Elliot

Resumo

As ligas de alta entropia (LAE) diferem das ligas convencionais devido ao seu número de elementos constituintes. Estas ligas conjugam 5 ou mais elementos com o objetivo de tirar partido das propriedades desses elementos num novo material. O tema desta tese aborda a LAE – CoCrFeMnNi – quando submetida a dois tipos de processamento a laser, unilateral (LAE 1) ou bilateral (LAE 2), o que afetará a microestrutura do material e, consequentemente, as suas propriedades.

O objetivo principal é perceber como o processamento a laser modifica a microestrutura das amostras e como elas se comportam após processamento. A estrutura do grão obviamente será afetada, portanto outro objetivo é estudar a sua evolução e efeito na dureza e nas propriedades mecânicas do material.

Foram realizados processamentos a laser, análises microestruturais, englobando microscopia óptica (MO) e difração de eletrões retrodifundidos (EBSD), testes de dureza de Vickers e, finalmente, testes de tracção aliados à análise de microscopia eletrónica de varrimento (MEV) das superfícies de fratura.

Resultante dos procedimentos descritos, as análises de MO e EBSD mostraram a abundância de grãos dendríticos colunares, com a presença de vários grãos refinados equiaxiais, numa estrutura CFC. O tamanho da granulometria obtida foi de 50~175 μm de comprimento, 5~45 μm de largura na LAE 1 e 40~150 μm de comprimento, 5~30 μm de largura na LAE 2 para os grãos colunares. Os grãos equiaxiais apresentaram um tamanho de aproximadamente 1~5 μm em ambas as amostras. Quanto à dureza, as zonas correspondentes ao material base apresentaram 320 HV e 230 HV para as LAE 1 e 2, respectivamente. Após o processamento, as zonas de fusão das amostras (ZF) tornaram-se mais macias (diminuição de 50~150 HV) e as zonas termicamente afetadas (ZTA) mais duras (aumento de 30~100 HV). Por fim, em relação aos ensaios de tração, observou-se que ambas as amostras são capazes de suportar muita tensão no regime elástico, 510-545 MPa, mas a LAE 2 tem maior capacidade no regime plástico, 660 MPa, em vez dos 560 MPa da LAE 1. Quanto à ductilidade, a LAE 2 também consegue alongar-se mais que a LAE 1 durante o mesmo ciclo de deformação. A extensão em fratura foi de 13 e 19% para as LAE 1 e 2, respectivamente.

Palavras-chave: ligas de alta entropia, processamento a laser, fabricação aditiva, ductilidade

Abstract

High entropy alloys (HEAs) differ from conventional alloys because of their number of element constituents. These alloys conjugate 5 or more elements with the aim of taking advantage of these elements' properties in one new material. The subject of this thesis addresses the high entropy alloy – CoCrFeMnNi – when submitted to two kinds of laser processing, one-sided (HEA 1) or two-sided (HEA 2), that will affect the material's microstructure, and consequently its properties.

The main goal is to understand how the laser processing modifies the samples' microstructures and how they behave after the processing. Grain structure will obviously be affected, so another objective is to study its evolution and effect on the material's hardness and mechanical properties.

Laser processing was carried out, microstructural analysis, including optical microscopy (OM) and backscattered electron diffraction (EBSD) were also performed, some Vickers hardness tests and, finally, tensile tests combined with a scanning electron microscopy (SEM) analysis of the fracture surfaces.

Resulting from the described procedures, the OM and EBSD analysis showed the abundance of columnar dendritic grain, with the presence of several refined equiaxed grains, in an FCC structure. The size of the obtained granulometry was $50\sim175\ \mu m$ length, $5\sim45\ \mu m$ width in HEA 1, and $40\sim150\ \mu m$ length, $5\sim30\ \mu m$ width in HEA 2 for the columnar grains. The equiaxed grains were sized $1\sim5\ \mu m$ on both samples. As for the microhardness, the base material areas had $320\ HV$ and $230\ HV$ for HEA 1 and 2, respectively. After processing, the samples' fusion zones (FZ) became softer (decrease of $50\sim150\ HV$) and the heat affected zones (HAZ) harder (increase of $30\sim100\ HV$). Finally, regarding the tensile tests, it was observed that both samples can handle a lot of stress in the elastic regime, $510-545\ MPa$, but HEA 2 is more capable in the plastic regime, $660\ MPa$, instead of the $560\ MPa$ by HEA 1. As for the ductility, HEA 2 can also elongate more than HEA 1 during the same deformation cycle. Fracture strain of 13 and 19% for HEA 1 and 2, respectively.

Keywords: high entropy alloys, laser processing, additive manufacturing, ductility

Contents

List of Figures

List of Tables

Acronyms

AM Additive manufacturing

BCC Body-centered cubic

BM Base material

BSE Backscattered electrons

DED Directed energy deposition

2D Two dimensions

3D Three dimensions

EBSD Electron backscatter diffraction

EBM Electron beam melting

EDS Energy dispersive X-ray spectroscopy

FCC Face-centered cubic

FZ Fusion zone

HAZ Heat affected zone

HCP Hexagonal close-packed

HEA High entropy alloy

OM Optical microscopy

PBF Powder bed fusion

SE Secondary electrons

SEM Scanning electron microscopy

SLM Selective laser melting

UTS Ultimate tensile strength

VEC Valence electron concentration

YS Yield strength

1

INTRODUCTION

1.1. What is a High Entropy Alloy?

A high entropy alloy (HEA) follows the same principle of a conventional binary or ternary alloy, but conjugates multiple elements in one alloy and they were introduced by Cantor *et al.* [1]. This kind of alloys will count with five or more elements with a concentration between 5 and 35% of each one [2]. The most common distribution of concentrations tends to be equiatomic, just like the one that will be studied further in this thesis – CoCrFeMnNi with 20 at. % of each element.

The study of HEAs can be a challenging theme because the conventional alloys that we are used to have taught us that, usually, when we add more elements to an alloy it will tend to a greater state of disorganization, forming intermetallic phases that can be unpleasant. As a solution, Yeh *et al.* [3] discovered that the combination of various elements in appropriate quantities could avoid the homogeneity and the formation of the intermetallic phases, stabilizing in a simple crystal structure like FCC, BCC or HCP rising the possibilities of taking advantage of this HEAs' properties [2], [4], [5]. High entropy alloys are mostly characterized by four main aspects that are expressed as physical effects. These are called "four core-effects" which can be resumed to:

- high-entropy effect for thermodynamics, related to the system configuration entropy
- sluggish diffusion effect, resulting in slower diffusion kinetics than in conventional alloys improving the high temperature properties
- severe lattice distortion effect caused by the presence of five atoms with different sizes
- cocktail effect when the addition of a specific element can significantly improve a specific property of the alloy

The "four core-effects" can also be associated to the great physical and mechanical properties of this kind of alloys, being able to satisfy a lot of applications' requirements at different temperature ranges (very low temperatures, as cryogenic levels, room temperature and high temperatures). These alloys are most often used as structural materials and they are of great interest to nuclear, marine, and aerospace industries [2], [4], [6].

1.1.1. As-rolled CoCrFeMnNi HEA

Furthermore, being the CoCrFeMnNi the most studied and common HEA [6] also known as Cantor alloy, it possesses very interesting properties as already mentioned earlier. It was the one chosen for the present work and investigation as it was originally rolled and will be laser processed later. The condition of as-rolled is obtained by submitting the material between rollers that will deform it into the desired final shape. This kind of alloys are almost always superior to any pure metal, alloy, or even bulk material because of their excellent behaviour under severe conditions or environments [4].

1.2. Fabrication and processability

Despite the Cantor alloy that has been addressed so far for its interesting mechanical properties, it still must be manufactured in a way that minimizes the need of processability. Some of the methodologies that must be considered are: arc melting, Bridgman solidification, atomization and laser cladding, all concerning the liquid processing approaches; the famous additive manufacturing (AM) that has been studied recently by several researchers and the most similar to the laser processing that will be used in this work; powder metallurgy associated to mechanical alloying; sputter deposition, atomic layer deposition and vapor phase deposition, as vapor state methods [7].

1.2.1. Additive manufacturing of HEAs

3D-printing or additive manufacturing is a recent method that has risen a lot of interest in the past years due to its ease of use and its way of producing parts. The most important advantage is the flexibility for producing irregular and complex parts since it uses a technique of covering layer-by-layer in each part. AM will be more efficient than the conventional assembly methods, since it is possible to avoid the step regarding the assembly of all components and it allows to simply obtain the final piece fully integrated.

There are specific processes for 3D-printing metals: binder jetting, sheet lamination, powder bed fusion (PBF) and directed energy deposition (DED). The most important ones for the development of HEAs are PBF and DED. PBF uses a laser or electron beam of high energy (associated to SLM or EBM) to melt the prelaid powder layer in a powder bed. DED can use the same associated laser or electron methods but also an electric arc to melt metal powders or wires during the printing path of deposition. These two methods are the most important ones due to their high heating/cooling rates which will shorten the interaction time of the applied energy with the metal powder and avoid the formation of intermetallic compounds. By refining the grain size of the microstructure this will result in improved mechanical properties [2], [8].

On the other hand, even though an appropriate fabrication method is a good starting point, a novel engineering alloy of interest shouldn't discard the processability methods like welding techniques. This is important because a HEA must be processable since there can emerge the need to work its shape structures and properties by coupling with another materials [9]. Due to the high strength and toughness that will be approached further, the high entropy alloys are difficult to machine or manufacture with complex structures. This fact gives even more emphasis and value to the additive manufacturing processes described above [10]. Thus, an illustration of the SLM processing setup is made in Figure 1.

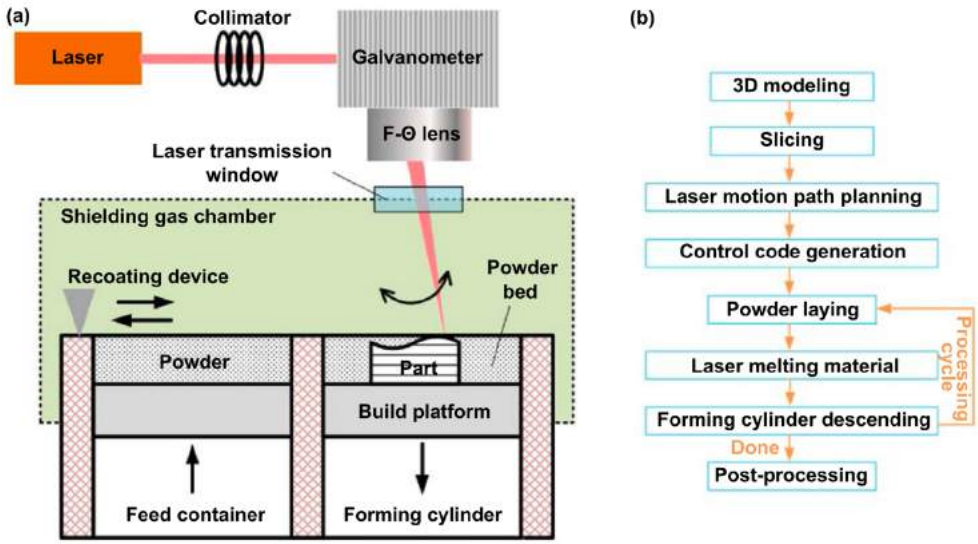

Figure 1 *– a) SLM processing setup; b) procedures for the SLM technique. Adapted from* [10]

A common SLM equipment is represented in Figure 1 and all the components necessary for the process are pictured in it. For better understanding, the most relevant components are the laser, a collimator to align the beam's direction, a shielding gas chamber, a forming cylinder, and a powder feeding system. The galvanometer is also very important since it works as an accelerated beam movement device so that the molten metal can easily melt and cooldown [10].

1.3. Phase evolution

When we study metals and metallic alloys, it is very important to consider their microstructure and respective phases. Since we are dealing with the "parent" high entropy alloy (CoCrFeMnNi), some studies and literature reviews have been made proving that this alloy presents a simple FCC structure with good ductility and fracture toughness properties [10]–[12].

The composition manipulation of the alloy takes an important role in this matter since it can drastically modify the lattice structure. For example, in the Cantor alloy an increase of Ni will contribute a lot for the FCC phase formation because of its high VEC (valence electron concentration). In HEAs the higher the VEC the easier is the FCC phase formation (VEC > 8) so, with a VEC of 10 Ni, we will have the described influence. In some cases, the post-treatment of the alloys, specially heat treatments, can promote alteration of the present phases.

Since we are focusing in the SLM process, Zhang *et al.* [10] performed SEM analyzes to study the density dislocations and sub-grain microstructure. Considering the cooling rate of 10^6 K s^{-1} it will result in high density dislocation which is usual in HEAs processed by SLM. This physical event can be avoided by submitting the material to an annealing process with high temperatures which can convert the elevated distortion energy into a low energy states lattice structure. Dislocation density will be a result of the accumulation of dislocation originated by the stress caused in the SLM process. Due to the high dislocation density a solidification substructure will be created inside the grain forming a sub-grain microstructure, contributing to the formation of a very refined grain, as shown in Figure 2.

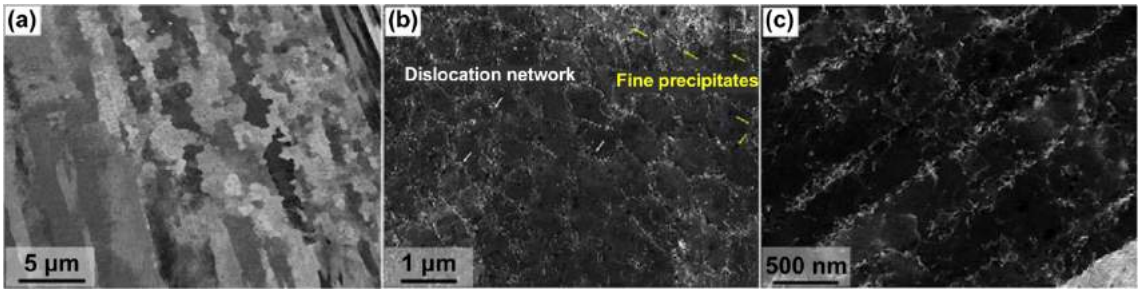

Figure 2 – SEM images for the CoCrFeMnNi HEA processed by SLM. a) high magnification backscattered electron (BSE) imaging of substructures; b), c) electron channelling contrast (ECC) images of dislocation networks and precipitates b) cellular structure and c) columnar structure [10]

The mentioned sub-grain microstructure can assume two different kinds of structures that are both represented in Figure 2, b) cellular structure or c) columnar structure. It is also noted in the image that there are dislocation networks representing the boundaries and that the dislocation density inside those substructures varied between almost none to filled with high density. Using the same annealing process as described before, it is possible to minimize the cellular substructure appearance and lower the dislocation density. As it is possible to observe in the same image, some precipitates were formed in the substructure boundaries which are a result of the SLM process [10].

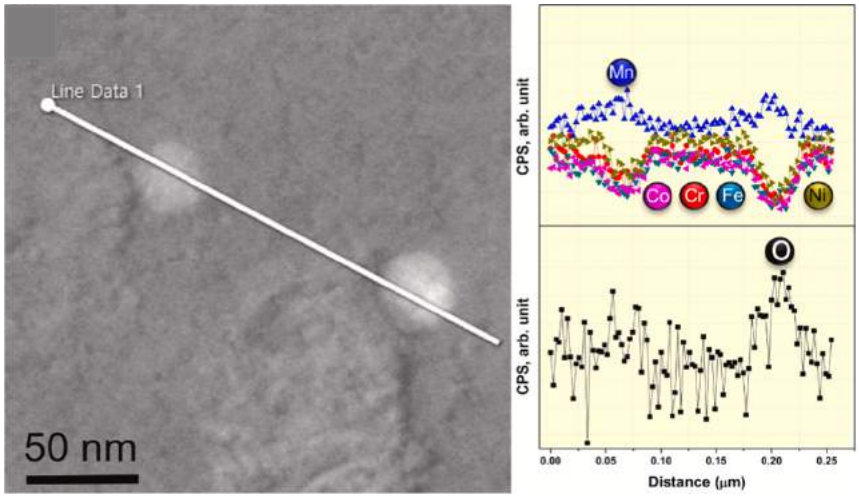

Figure 3 – TEM and EDS analysis on the CoCrFeMnNi HEA after SLM [13]

Those precipitates existence can also be confirmed by the work of Y.-K. Kim *et al.* [13] who carried an EDS profile analysis which detected the presence of 2nd phase particles (Mn and O) in the compound. Together they form the Mn_2O_3 oxide that was noted by the precipitates. For great surprise, these precipitates would turn out to be beneficial for the alloy since they can reinforce it and prevent the grain coarsening during heat treatments [13].

1.4. Physical and mechanical properties

1.4.1. Main properties and manipulation

As it has been referred along this work the high entropy alloys present great potential when it comes to mechanical properties for practical applications because of their high performance and commitment between strength and toughness. This kind of materials could represent the metals' next generation because of its already known physical and mechanical properties at extreme conditions, but also because of the undiscovered properties that are still to be found [10].

Concerning the determination of these properties it should always be considered that the constituent elements, processing conditions and work temperature play an important role in this matter, as well as for the mechanical manipulation of the alloy when it is needed. Sometimes, heat treatments (mostly annealing) are performed when the wanted properties are not achieved but we should keep in mind that the grain coarsening will negatively affect the yield strength and tensile properties of HEAs [8].

J.P. Oliveira *et al.* [6] carried out a study about the mechanical properties of a Cantor alloy in comparison with an as-welded alloy with the same constituents. Some of the mechanical properties are presented in Table 1 where the base material is equivalent to our as-rolled CoCrFeMnNi HEA.

***Table 1** - Cantor HEA mechanical properties summary*[6]

Reference	*Yield strength (MPa)*	*Ultimate tensile strength (MPa)*	*Fracture strain (%)*
Base material	587 ± 7	943 ± 6	9.5 ± 0.2
CoCrFeMnNi welds	248 ± 4	519 ± 3	8.4 ± 0.4

Regarding their results it is possible to say that in a welding scenario this alloy will reduce its main strength and ductility once it was submitted to high temperatures that result in large grain size microstructures [6].

Our HEA possesses several of the usual corrosion resistant elements, as Co, Cr and Ni, allied to literature results that obtained better corrosion resistance in HEAs than in conventional high-corrosion-resistant alloys [14]. Thus, it is expected that the CoCrFeMnNi alloy presents a very interesting behaviour when submitted to oxidizing media.

1.4.2. Influence of SLM method on HEA's properties

Apart from the difficult machinability that comes from general high entropy alloys, the AM process (mostly from selective laser melting), on the other hand, can improve the property of wear resistance. These alloys will become difficult to machine but present great wear resistance, which can be justified by the refinement of grain that happened during the SLM process. This will lead to the use HEAs for surface cladding, for example [10], [15].

All this importance that is being given to AM and SLM comes from the fact that it is the most similar method to the laser processing that will be done in this work. Also, because the mechanical properties that it includes present much better results and values than in the other processing methods, like laser melting deposition, powder extrusion, casting, etc. The main advantage of SLM over the other processes is the strengthening mechanisms that the material can follow without needing a post heat treatment, but to use this as an advantage on HEAs it must be very well supervised. Due to the coarse grains, dislocations, and low number of interface defects, even though showing better elongation values, those other processes will always need a post treatment to improve strength, but still getting worse performances than SLM [10].

The process of EBM (electron beam melting) is a competitor to SLM, but it still provides worse tensile properties than the last. The refined crystal granulometry and

uniform composition that avoids the formation of intermetallic compounds can justify the use of SLM instead of EBM. Regarding the yield strength it is influenced by the grain size and follows the Hall-Petch equation:

$$\sigma_y = \sigma_0 + k/d^{1/2} \quad \textbf{(1)}$$

The present variables on equation **(1)** represent, respectively, σ_y the yield strength, σ_0 the friction stress in absence of grain boundaries, k a constant and d representing the actual grain size [8].

1.5. Applications

1.5.1. Importance of AM in HEAs' applications

As it was earlier mentioned, in general the high entropy alloys are good structural materials and could be very important in some industries: aerospace, marine, energy, transportation, electronics, biomedical, and tooling sector. This is due to their superparamagnetic and superconductivity properties allied to the great mechanical performance under severe temperature ranges [4], [8]. More specifically, these advanced alloys are very versatile since they can work as hydrogen storage materials, radiation resistant materials, diffusion barriers for electronics, electromagnetism shielding materials, biomedical coatings, among others.

All these interesting applications could be enhanced if the mechanisms of manufacture and processing were simpler and more efficient. In accordance with the present work, all the specifications and parameters involved in AM picture it as one of the best methods to keep this commitment. The customizable properties, complex design freedom, and rapid heating/cooling rates provided by 3D printing will result in the refined microstructures that were already addressed and will support these applications. Other casting or processing methods show inferior mechanical properties as well as worse efficiency [8], [15].

1.5.2. Specific application for Cantor alloy

An example of a specific application for the Cantor alloy is its capacity of acting as a catalyst. While being thermodynamically metastable these alloys are also very resistant under corrosive environments. Some HEAs have been tested and CoCrFeMnNi showed good efficiency to degrade the azo dye (colorant organic compound), which is commonly associated to an atomic structure with severe lattice distortion. The porosity of 3D printed structures in HEAs has proved itself to enhance catalytic activity when compared to the 2D products. By increasing the superficial area of these porous structures it is possible to improve the catalytic activity even more [8].

As it was explained before, there are a lot of industries that could use the help of HEAs because of its mechanical capabilities and temperature handling. Thus, in the following practical work, some of their competences will be tested with the objective of complementing the works that are already in the literature.

2

MATERIALS AND METHODS

2.1. Laser processing

The processing of the HEA by laser was a work done by professor João Pedro Oliveira in Canada and then shipped to Portugal, where its study would be performed in NOVA. For this matter, samples were separated into two groups: HEA 1 and HEA 2, which were distinguished by the different kind of processing that was applied to each group. HEA 1 was hit with the laser just on one side while HEA 2 on both sides, as it is shown in Figure 4. The laser was applied in pulses and the chosen power was 1,15 kW. Each pulse had a time of exposure of 10ms and an overlap of 25%. All the materials and methods used in our laboratories will be described further in this chapter.

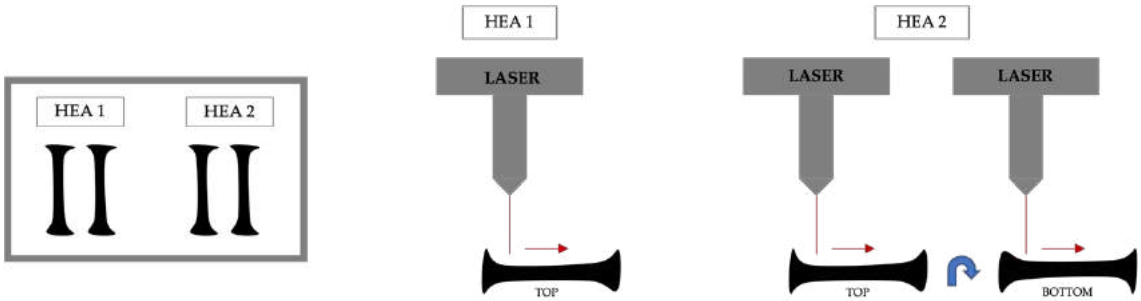

Figure 4 *– Representative schematic of laser processing*

2.2. Surface polishing and chemical etching

Since the samples were already laser processed, the first experimental procedure to be done at the university laboratories is their preparation and mounting in an Epoxy resin. After this, the surface polishing can start and the samples follow the evolution of the polish papers granulometry, starting from P320 and ending in the P4000 SiC paper, as shown in Appendix A2. Before advancing to the microstructure analysis, it is essential to remove the last small scratches with a diamond compound and then immerse the samples into an etching solution of Kalling's-2 at room temperature [16],[17] with a duration time of around 100s. All the polishing was done using a Buehler Phoenix Alpha polisher machine (Appendix A1). Before changing to a new SiC paper, each microstructure was observed using an Olympus CX40 optical microscope, but the final microstructures were visualized and photographed using a Leica DMI 5000M inverted optical microscope which has higher quality and much more accuracy.

Furthermore, an EBSD analysis was performed by a JSM-7100F and Helios Hikari UMSII in Korea to complement the microstructural evaluation of our samples. The TSL OIM Analysis 7.0 software was used to process the raw EBSD data.

2.3. Microhardness testing

The next step on the experimental procedures is to test the microhardness of our samples. This testing can only be made after finishing the polishing and respective etching. The kind of microhardness in cause is the Vickers Hardness and experiments were made using a machine like in Figure 5, a Mitutoyo HM Hardness Testing Machine. Two groups of fusion zones affected by the laser processing were chosen to be tested and the adopted parameters for this matter were: a force of 0.2kN, 0.15mm between each indentation (vertical and horizontally), and 10s for the time of indentation. All this resulted in a total of 160 indentations for each group in the fusion zones.

All the data provided by the machine was saved to an Excel sheet and later treated to get results and find conclusions about the hardness of these samples. Some Contour graphs were obtained through OriginLab software so that it becomes easier to compare the values of hardness.

***Figure 5** – Mitutoyo HM Hardness Testing Machine*

2.4. Tensile tests

Since some of the mechanical properties are still to be determined, the tensile testing was conducted as a final step of the practical work. Traction tests were performed using a Shimadzu tensile machine with a 50kN load cell. Both kinds of samples (HEA 1 and HEA 2) were submitted to this longitudinal testing and the chosen parameters were the room temperature and a tensile rate of $1x10^{-3}s$. Tests were undertaken until the moment of fracture in both samples, using adequate test pieces that were cut just for this purpose.

After the fracture, the respective results and graphs for each sample were saved for later interpretation.

Finally, when all the tests were finished it was necessary to analyse the fractured surface of our samples. This step was made using a Hitachi SU3800 which is a scanning electron microscope (SEM) in the mechanical engineering department at NOVA SST. All the obtained images will be presented in the following chapter.

3

RESULTS AND DISCUSSION

3.1. Microstructural analysis

3.1.1. Optical Microscopy

Since the experimental procedures started with the surface polishing and respective chemical etching, it makes sense to start the discussion with the results of these actions. Polishing was the first step as it is very important to remove all the surface scratches. Then, the chemical attack was performed so that the microstructure became visible. This way, the two kinds of samples were characterized by OM as it is possible to observe their microstructures in appendices B and C. Further, through zoomed images of the obtained microstructures (Figures 6, 7 and 8), the refined grain with dendrites can be seen clearly below. Moreover, the determination of their length and width was also performed, obtaining values of $50{\sim}175\,\mu m$ and $20{\sim}70\,\mu m$, respectively, for the columnar grains of HEA 1.

In what HEA 2 is concerned, its grain dimensions were also determined. This group of samples had a small difference because it was laser processed on top and bottom (see Appendix C) instead of just on top, like HEA 1. The dominating type of morphology is also the columnar dendritic, as we can see in Figure 7.

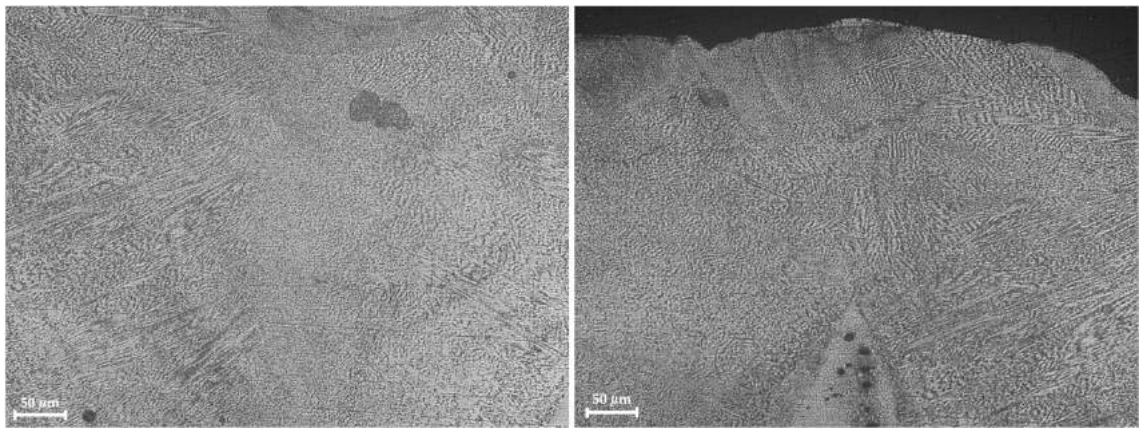

Figure 6 *– Zoom of fusion zones from the microstructure images of HEA 1 to visualize the dendrites and grain size*

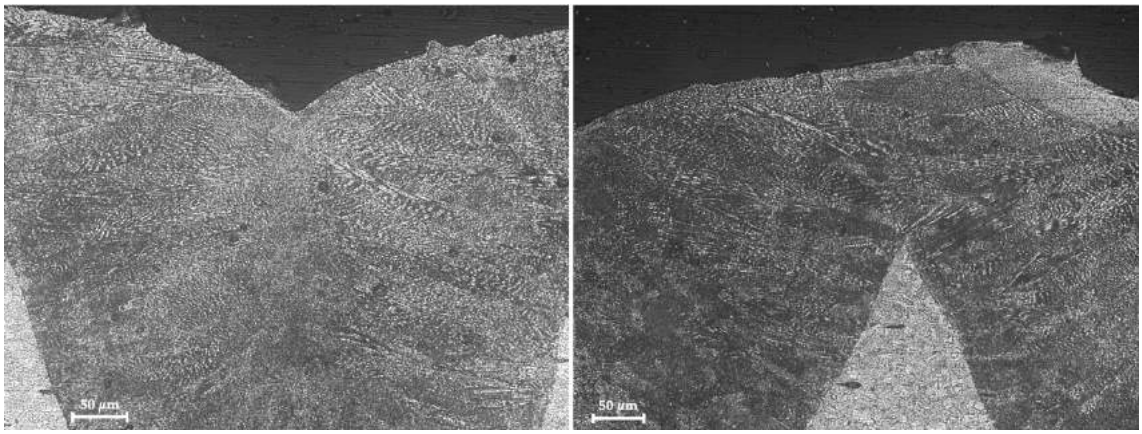

Figure 7 *– Zoom of fusion zones from the microstructure images of HEA 2 to visualize the dendrites and grain size*

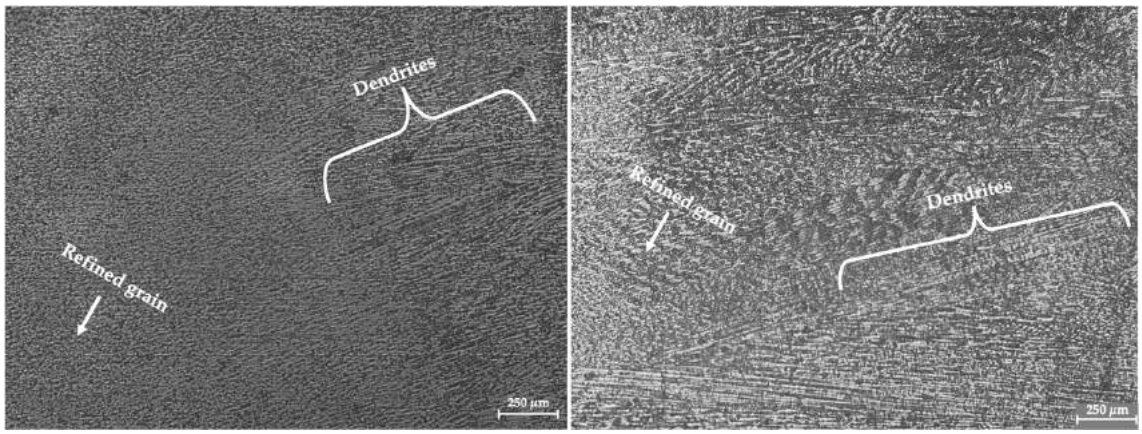

Figure 8 *– Identification of specific zones of the microstructure to observe dendrites and the refined grain in detail. HEA 1 represented on the left side and HEA 2 on the right side of the image.*

By analysing the previous images, the measured length and width for HEA 2 were respectively $0.150{\sim}2\ mm$ and $50{\sim}150\ \mu m$. As it was mentioned before, in both groups of samples there can also be noted the presence of a lot of very small equiaxed grains ($1{\sim}5\ \mu m$) which will contribute to get improved hardness values and mechanical resistance. These are some of the most important properties that characterize HEAs, and which were already addressed in the Introduction to this thesis [18].

To support these results and conclusions, emphasizing the dendritic shaped granulometry, zooms in certain spots were made for each sample to help identify this granulometry, as we can see in Figure 8.

As shown in Figure 8, the presence of dendrites and refined grains is observed in both samples. Even though these two kinds of grain are visible, we can also observe that in HEA 1 there is a significant amount of refined grains and less dendrites, but in HEA 2 the opposite happens. It is possible that this results in a greater microhardness for HEA 1, but this should be confirmed further ahead.

Hongge Li *et al.* [20] and S.A.A. Shams et al [21] also performed some studies about the Cantor alloy and its microstructure, so it is possible to say that the obtained values are in accordance with these works. Another work related to the SLM process in which we can rely on is the Bowen Wang *et al.* [22], along with the Hongge Li *et al.* [20] constitute a summary table (Table 2) with the obtained values of granulometry to confirm the results of the present work. Also, by observing appendices B and C, it is possible to identify the presence of pores in both samples and this can be justified by the presence of Oxygen impurities forming oxides [23].

Table 2 *– Grain size comparison between the present work and the literature*

Granulometry

	Dendritic		**Equiaxed**
	Length	**Width**	
Hongge Li et al.	20~160 μm	15~75 μm	~7.5 μm
Bowen Wang et al.	100~400 μm	30~100 μm	~500 nm
This work	0.05~2 mm	20~150 μm	1~5 μm

3.1.2. Electron backscattered diffraction

EBSD analysis is also a very commonly used method to characterize the microstructure. As so, the samples were analysed by EBSD and the results are presented further below. In appendix D there is an example of mapped zones in the HEA 1 sample.

Regarding the first kind of processing, some of this sample's peaks can also be observed in appendix D where all the different zones (BM, HAZ and FZ) are mapped and can be distinguished. The first two highlighted areas were chosen and zoomed in to demonstrate with better precision an example of a welded joint and a fusion zone, which are represented in Figure 9.

Regarding the distribution of the five elements, the surface looks very homogeneous, as in the work of Przemyslaw Litwa *et al.* [19], and organized in an FCC structure, as predicted in the literature review [19].

Since the preferred lattice orientation for the grain growth in this material is the <111> [21] as for the processed material in Figure 9-A, EBSD analysis provides us information about how the grains are organized in the different areas of the material. In the welded joint, since the same parameters were used and the welding happens to be joining the same kind of material, its microstructure looks very homogeneous and corresponds to the close-packed <111> FCC structure that rules these alloys [19].

Columnar granulometry in the FZ is predominant and can be confirmed once it prevails in all EBSD data, as it was also predicted before. Analysing the deeper zones of the sample in Figure 9-A, starting with the BM, it mixes the columnar and equiaxed granulometry with a hard but less packed structure, somewhere near the <111> and <101> lattice planes. The HAZ presents a very small equiaxed grain that starts to abound in a <001> structure, which will result in the hardest region of the sample [21].

Regarding Figure 9-B, it represents the middle of one peak, so it is possible to observe the evolution of the FZ.

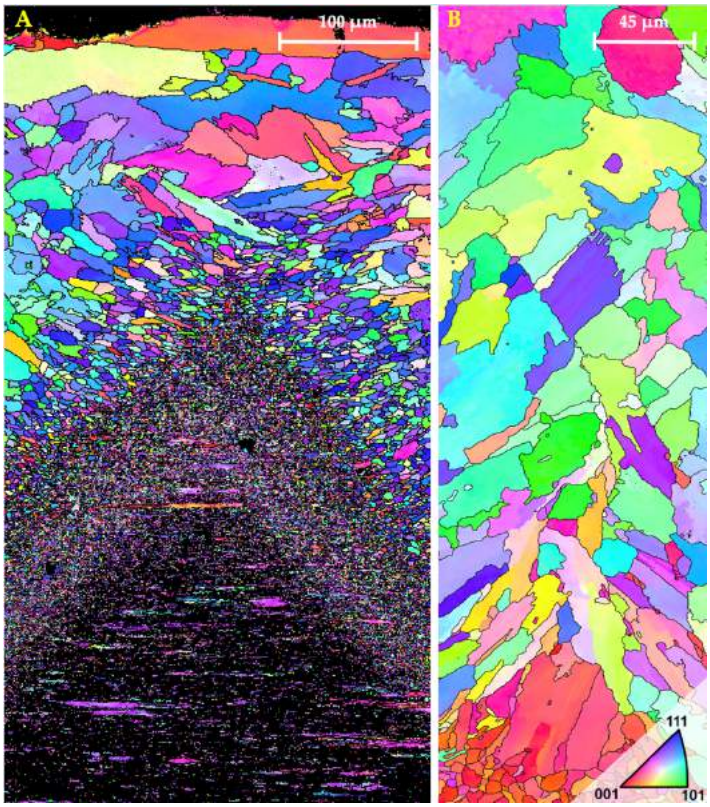

***Figure 9** – EBSD mapping of specific areas in HEA 1. A) Welded joint area; B) Fusion zone area.*

Further analysing deeper zones of the sample, in Figure 10 it is possible to visualize one of the heat affected zones that experienced grain growth. This figure also represents the third highlighted area (zone C) in appendix D, which goes further than the FZ and zooms in the direct HAZ of one peak. Under the effect of the thermal cycle induced by laser, the grain in this area has grown considerably, as it was already mentioned.

This grain evolution can be justified by the recrystallization that the BM's cold rolled grain suffered with the high temperature trigger, but also by the decrease of dislocation density [24].

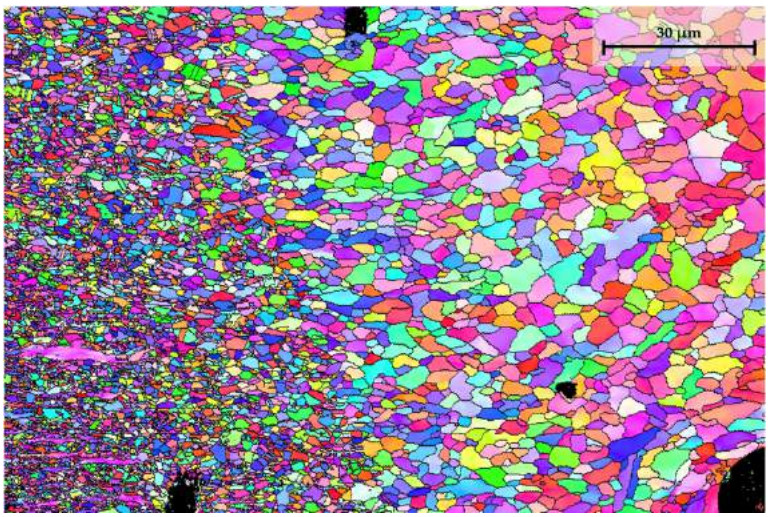

Figure 10 *– Zoomed image of a HAZ in HEA 1 experiencing grain growth.*

3.2. Microhardness analysis – Vickers hardness test

Regarding the microhardness analysis that was proposed for this thesis, the used methodology was the Vickers hardness testing. Experiments were made with the already mentioned parameters (on subchapter 2.3.) and the treated results provided graphs that will be presented and discussed below.

This kind of testing was only made after polishing and etching since the microstructure should be already visible when this is made in order to identify the spots of higher and lower hardness. This way, we will be able to relate the values of hardness comparing the location of the indentations in the laser welds.

As we already know the microstructure and the laser welds' locations, in Figure 11 it is possible to see the areas where indentations were made in HEA 1 (left) and HEA 2 (right).

After having finished all the indentations on both samples, it was necessary to analyse the obtained data. For this matter, beside the Excel sheet where the data was saved to, the values were then submitted to the OriginLab software which can provide us with "Contour Plot" graphs. This will make the visualization of the hardness values much easier due to the presence of various colours and the laser weld areas will be very clear.

Further below it is possible to observe the mentioned graphs in Figures 12 and 13 relative to HEA 1 and HEA 2, respectively. One of the most evident conclusions about hardness is that, in general, at first sight HEA 1 is harder than HEA 2, as it is possible to see by comparison of both images (Figures 12 and 13). Specific values will be presented further below. This was also predicted in the microstructural analysis.

Another difference between the two samples which is also notable in the following images is the kind of processing in each of them. The incidence of the laser on just one side of HEA 1 is perfectly visible in Figure 12 but the two-side incidence in HEA 2 is not that easy to visualize in Figure 13. Once this sample was processed on both sides the HAZ will be very large because each top weld will affect the bottom one. Of course, the FZ will be the softest area on both samples and the less heat affected zone of HEA 2 will be in the middle of sample, where the values of hardness are less likely to change.

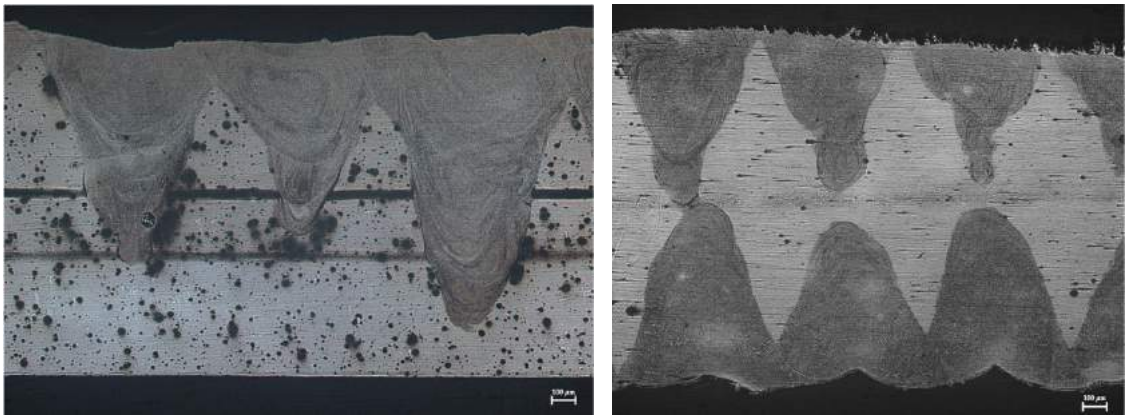

***Figure 11** – Areas where the Vickers Hardness Tests were performed. HEA 1 on the left and HEA 2 on the right side of the image*

For a better and more accurate evaluation of the obtained values of hardness the areas where the laser was applied were separately analysed. A comparison between the spots where the laser welds are present and the base material areas is made in Table 3. When the base material was mentioned, it cannot be just the base material because when a laser is applied to a sample, besides the FZ, there will always be a HAZ, which will also affect the material´s properties and, in this case, the values of hardness. These values are shown in the table below.

Table 3 *– Variation of values of hardness in the FZ and in the HAZ*

	HEA 1	***HEA 2***
FZ	188.4 – 278.2 HV	152.2 – 235.0 HV
HAZ	210.7 – 438.9 HV	172.1 – 245.3 HV
BM	~ 320 HV	~ 320 HV

In this work, due to the small size of the analysed samples and the way the laser processing was performed, the HAZ will cover almost all the samples' areas that seem unaffected. As so, it is probable that we won't have unaffected base material areas to compare values with. As for HEA 1, it is possible that the extreme end of the piece that was not hit with laser could have been unaffected by the heat and so preserved the base material's hardness, with a value of approximately 320 HV.

The HAZ of HEA 2 will be larger than in HEA 1 because of the laser processing on top and bottom which will double the incidence of heat on this sample. Due to that fact and allied to the shown graphs and the obtained values it is possible to justify the lack of hardness by HEA 2 in comparison to HEA 1, with the knowledge that they were produced at the same time and with the same parameters.

By analysing the previous results and grounded on the literature review, it is possible to support the obtained values and to confirm the drawn conclusions. As predicted before and in accordance with the variation of grain size, the zones of equiaxed grains present a much higher value of microhardness than the columnar zones [25]. This also happens to be justified by the refinement of grain which is similar to the one observed in the work of Hongge Li *et al.* [20].

Regarding the overall microhardness of our as-rolled HEA 1, which is the one that for sure preserved some BM properties, its value of ~320 HV seems to be in conformity with the obtained 350 HV in [26].

It is worth to mention that the values of hardness in the HAZ are plausible, even with the remarkable difference between HEA 1 and 2 that has already been addressed. The recrystallization induced by the latent heat justifies the increase of strength and hardness in this zone [26].

Another support to our results is the work of J.P. Oliveira *et al.* [24] which studied laser welds in the same kind of HEA as this thesis. They concluded that the hardness in the CoCrFeMnNi end was approximately 173 HV and the fusion zone that joins with the stainless steel had 220 HV of hardness. These values can be compared to the ones obtained in this work and, as it is possible to see in Table 3, they seem to be in accordance.

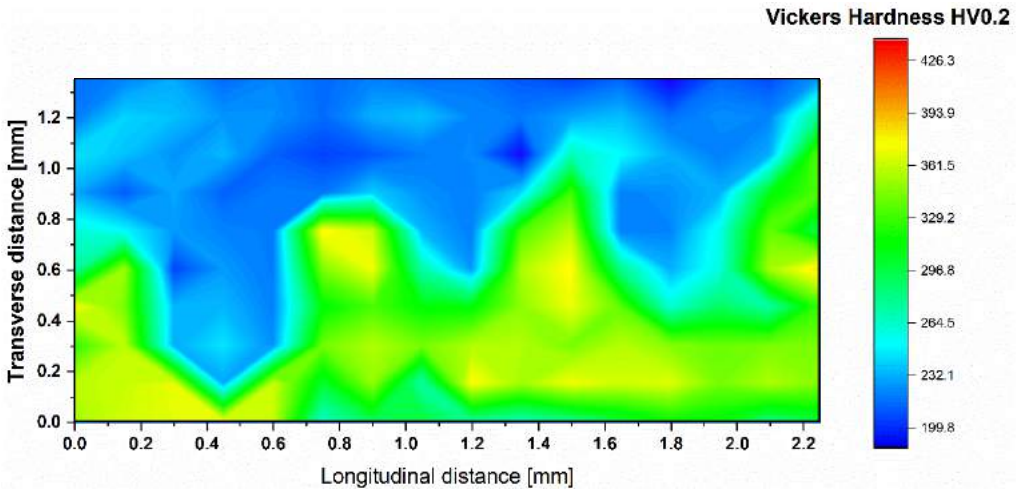

Figure 12 – Microhardness mapping using a contour plot from OriginLab for HEA 1

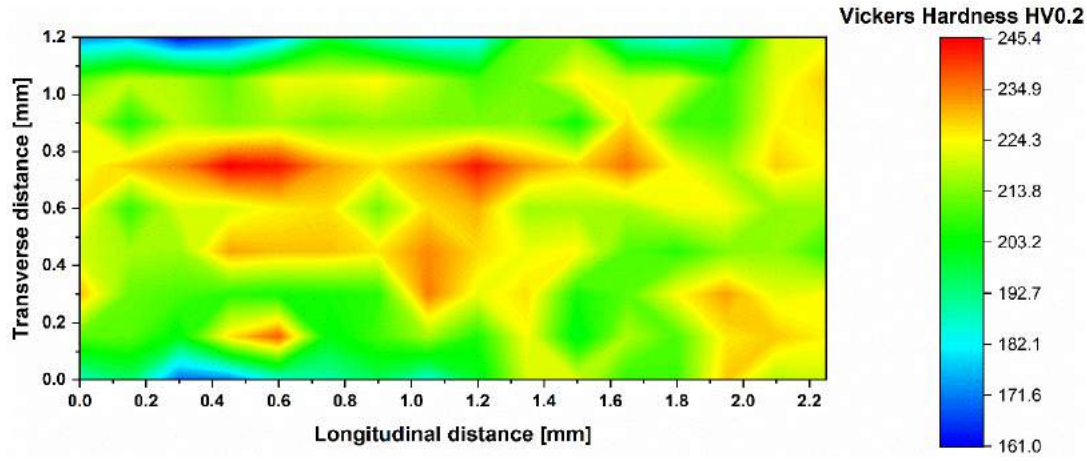

Figure 13 – Microhardness mapping using a contour plot from OriginLab for HEA 2

3.3. Tensile testing – Tensile loading until failure

The tensile tests complete the mechanical characterization of our samples and represent the final step of the practical work in this dissertation. Since this kind of tests are very versatile in providing a lot of different data, properties like ultimate tensile strength (UTS), yield strength, elongation, Young's modulus, among others, are just some of those that are possible to determine in this testing.

With the aim of establishing a relationship between the mentioned properties and the kind of processing that each HEA 1 and HEA 2 was submitted to, the same parameters were applied during tensile testing. As so, in the end of these tests we should be able to understand the strength limits of our alloys.

Since the main properties were already addressed before, it is time to explain how to determine them. For better interpretation of the following graphs, we should be able to identify two different regions.

On one hand, depending on the ductility of the material and representing the first part of the graphical curves, there will be the elastic region until the point of yield strength. From this point, we will observe the plastic region, in which the material starts to give in until the moment of its complete fracture. As so, YS is the highest point in the elastic region, UTS is the highest point of the whole curve and the Young's modulus is commonly determined by the slope of the elastic region [27].

3.3.1. Graphical results

All the described parameters were applied to our tests in HEAs and all their respective data was provided by the utilized tensile machine.

For the sample with one punctured side by laser (HEA 1), that is the less heat affected one, we start to analyse its properties with the help of the stress/strain graph, shown in Figure 14, which also presents some noise on the curve due to the incidence of the laser that induced the formation of a more heterogeneous material.

The fracture of this sample happened when the strain was at 12.5%, but the material could still handle some significative plastic deformation. We can say that this sample behaves as elastic as plastically during its deformation.

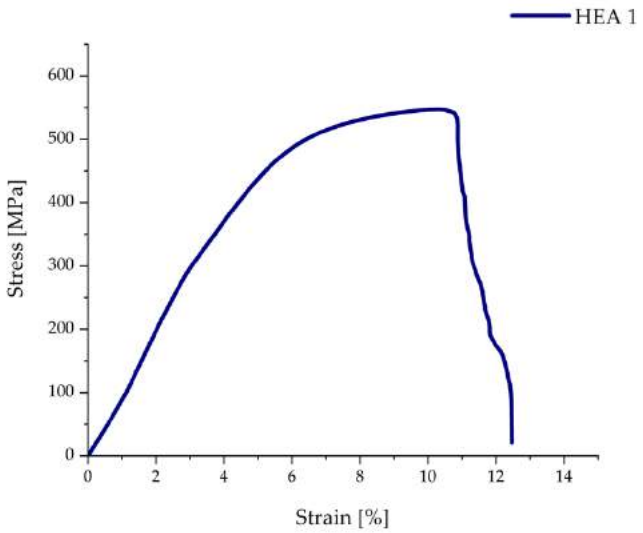

Figure 14 *– Stress vs. Strain graph for HEA 1 as a result of the tensile tests*

Regarding HEA 2, as already mentioned above, this sample was also submitted to the same tensile tests as HEA 1 so that a comparison between both can be made, and conclusions can be drawn about the laser processing.

A second stress/strain chart was produced as shown in Figure 15, this time for HEA 2. Just by observing the two graphs it is possible to note a clear difference between the kind of curve in each of them. Thus, it is obvious that the elastic and plastic behaviour of this sample will be very different from HEA 1.

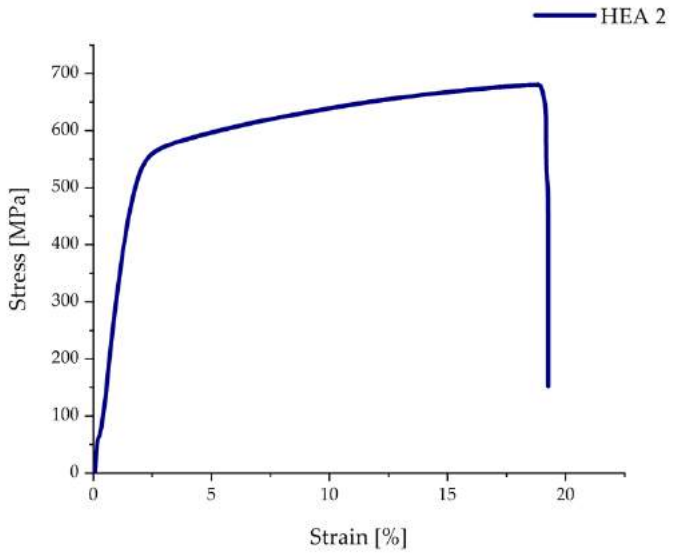

Figure 15 *– Stress vs. Strain graph for HEA 2 as a result of the tensile tests*

For an easier interpretation of all the obtained data, a summary table (Table 4) was produced to compare the two different samples under study. This table establishes a comparison between HEA 1 and 2 regarding the values of yield strength, ultimate tensile strength, and moment of fracture.

In terms of handling stress before plastic deformation, both samples show equivalent values of yield strength, with HEA 2 slightly more capable.

Differences begin in the UTS values where HEA 2 is also more capable to handle stress before fracture than HEA 1 but, this time, the difference is much higher.

The most evident disparity between both is the already mentioned elasticity, that it also reflected in the graph of Figure 14, and which can be considered remarkable for HEA 1. On the other hand, HEA 2 is a rigid sample that can handle a lot of plastic deformation which will help in the delay of the material's fracture.

Table 4 *– Summary table with the tensile tests' results*

	HEA 1	***HEA 2***
YS	(not accurate)	545 ± 7 MPa
UTS	550 ± 13 MPa	690 ± 8 MPa
Fracture strain	12.5 ± 0.2 %	19 ± 0.4%

According to J.P. Oliveira *et al.* [24], continuing his previous work [26] about the welding of a stainless steel with the same kind of HEA used in the present work, plastic deformation should preferentially occur in the FZ because of the large equiaxed grains that result in a lesser hard region. With larger granulometry in this area there will be higher dislocation density in the boundaries, so the material tends to deform first here. This can explain the huge difference between the plastic regions' sizes in HEA 1 and 2.

HEA 1 has a small HAZ, which results in a small FZ when compared to HEA 2. As so, due to the double incidence of the laser in HEA 2, its FZ is much larger and more homogeneous. This homogeneity and grain size result in less boundaries so it becomes easier to deform plastically, allowing this sample to deform in an interesting way.

Comparing the data in the previously mentioned articles with the summary table in this work, it is possible to take some conclusions about the effect of the laser processing in CoCrFeMnNi. Since the base material has a YS of 587 MPa, UTS of 943 MPa and the fracture occurs at 9.5% of strain in [26], it is possible to say that without significant reduction of the YS, both samples show an increased ductile capacity, specially HEA 2. Regarding the maximum stress that they can handle before fracture (UTS), a 45 to 65% decrease is noted when the laser processing is performed.

All these results showed interesting properties that could be applied in the future, and, once again, gave credibility to this kind of laser processing. Everything seemed to be in accordance with the expected (AM), knowing that the expected was not exactly the same kind of processing in this work. Nevertheless, both samples exceeded expectations in what elastic behaviour is concerned.

3.3.2. Fractured surface analysis – SEM

For the conclusion of the programmed practical work, as explained in the chapter of Materials and Methods, after the moment of fracture in the tensile tests it is necessary to observe the samples' surfaces. As so, scanning electron microscopy was used due to its 3D high magnification capacity allied to a great resolution. [28] All the following images were obtained with the incidence of SE, except for the Figure 16-A that was obtained with BSE.

In the first image presented below (Figure 16), the fractured surface of HEA 1 is analysed where some properties or defects are visible and can be explained. The most important properties are the ones shown in Figures 16-B and -C which allow us to visualize two opposite properties in the same sample, 16-B is an example of ductile features, while 15-C of brittle-like features. Nonetheless, the majority of the fracture surface is composed by many small dimples.

Even though HEA 1 shows a few little fractures that represent the regions of brittleness, we cannot consider that it is a fragile sample, since the most prevalent property is ductility, as detailed in the stress-strain curve and further corroborated by the presence of dimples.

For the HEA 2 surface fracture analysis, the same kind of imaging (SEM) was used, and the fractured surface is visible in Figure 17.

Due to the obtained graphical results, before observing the surface, it was already possible to understand that HEA 2 is a much more ductile sample than HEA 1, since it has a higher value of elongation. All the visible dimples in Figure 17-C confirm the high ductility obtained in the graphical results. These dimples show that the ductile behaviour prevails, and there is no evident sign of brittleness in this sample.

All the obtained results seem to be in accordance with the work of J.P. Oliveira *et al.* [24] that is related to the Cantor alloy, and which was also tested until its fracture. The described dimples and the presence of some brittle spots on the samples of this thesis are similar to the ones mentioned in the work of J.P. Oliveira. On the other hand, although the kind of fracture observed in these two works is identical, the present work showed improved values of stress and strain when compared to the welding with a 316 stainless steel.

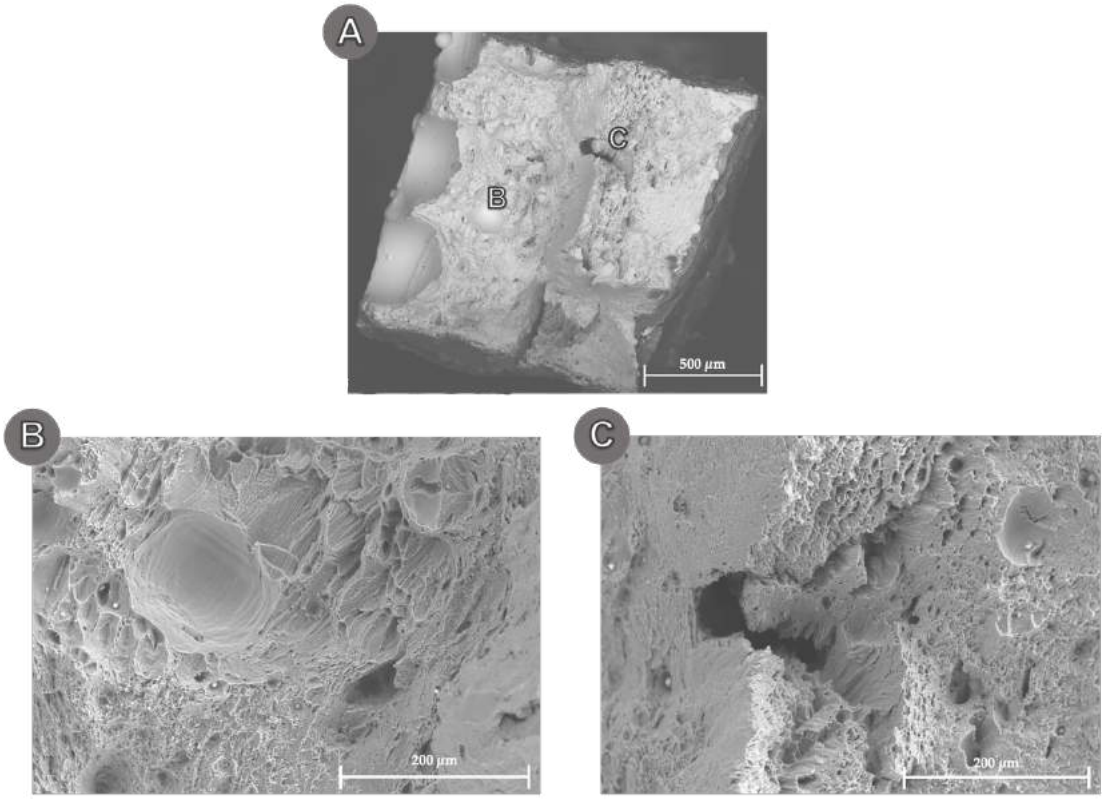

Figure 16 *– SEM images from HEA 1's fractured surface. A) Identification of two different fractured zones; B) Zoomed area that represents the plasticity of the material; C) Zoomed area that represents the brittleness of the material.*

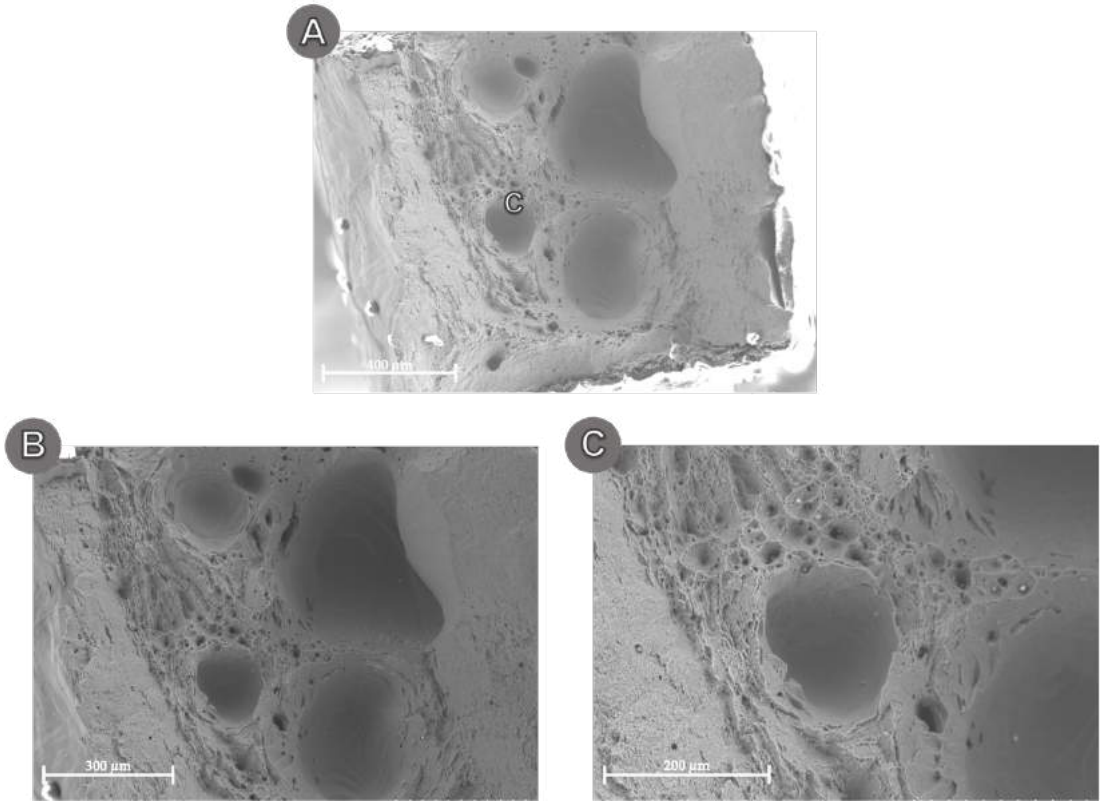

Figure 17 *– SEM images from HEA 2's fractured surface. A) Visualization of the fracture behaviour; B) Zoomed area of the most affected spots; C) Close-up in a material's failure.*

4

CONCLUSIONS

Since the Cantor alloy has already proven its interest as a structural material with great mechanical properties and very good temperature handling, both under high and low temperatures, a laser processed sample of the same kind was studied in this thesis and its achievements will now be addressed.

Following the presented work, the first accomplishment was about the microstructure evolution which showed a similar behaviour to an as-rolled Cantor alloy. Columnar dendritic and equiaxed granulometry in an FCC structure, as predicted in the literature, but the laser processing ended up refining even more the grain. The length and width sizes for the columnar grain were respectively $50{\sim}175\ \mu m$ and $5{\sim}45\ \mu m$ for HEA 1, $40{\sim}150\ \mu m$ and $5{\sim}30\ \mu m$ for HEA 2. Equiaxed refined grains were sized $1{\sim}5\ \mu m$. Through the EBSD analysis it was possible to confirm the presence of the close-packed FCC structure and to identify the microstructure's different areas (BM, HAZ and FZ) with different grain evolution.

Then, concerning the microhardness tests, one of the most visible results was the fact that HEA 1 is harder than HEA 2, with a difference of $100{\sim}150\ HV$, so the most heat affected sample lost some hardness capabilities. The highest difference between the two samples was associated to the HAZs, since the second sample experienced higher values of temperature, resulting in grain coarsening and so becoming softer. As in the work of J.P. Oliveira *et al.* [26], the high values in the HAZs resulted from the recrystallization induced by the latent heat in those zones.

Regarding the performed traction tests that provided information about our samples' tensile properties, they both showed an improved ductile capacity, with HEA 2 almost reaching 20% of fracture strain. HEA 1 demonstrated a better behaviour in the elastic regime and HEA 2 handled more stress in the plastic regime. Comparing with the literature, the obtained values of YS were nearly equivalent, but the UTS ones suffered a decrease of 45 to 65% after the laser processing. Through the SEM images of the fractured surfaces the high ductility was once again confirmed on both samples by the visible dimples.

Finally, as a proposal for future investigation of these alloys, a series of heat treatments to understand how the as-rolled CoCrFeMnNi relates with the laser processed samples could be conducted. After the heat treatments, samples should follow the same experimental path done in this thesis to establish a comparison with the results of this work and with additive manufactured samples.

5

REFERENCES

[1] B. Cantor, I. T. H. Chang, P. Knight, and A. J. B. Vincent, "Microstructural development in equiatomic multicomponent alloys," *Mater. Sci. Eng. A*, vol. 375–377, no. 1-2 SPEC. ISS., pp. 213–218, 2004, doi: 10.1016/j.msea.2003.10.257.

[2] P. Chen, S. Li, Y. Zhou, M. Yan, and M. M. Attallah, "Fabricating CoCrFeMnNi high entropy alloy via selective laser melting in-situ alloying," *J. Mater. Sci. Technol.*, vol. 43, pp. 40–43, 2020, doi: 10.1016/j.jmst.2020.01.002.

[3] J. W. Yeh *et al.*, "Nanostructured high-entropy alloys with multiple principal elements: Novel alloy design concepts and outcomes," *Adv. Eng. Mater.*, vol. 6, no. 5, pp. 299–303, 2004, doi: 10.1002/adem.200300567.

[4] J. Li, X. Meng, L. Wan, and Y. Huang, "Welding of high entropy alloys: Progresses, challenges and perspectives," *J. Manuf. Process.*, vol. 68, no. PA, pp. 293–331, 2021, doi: 10.1016/j.jmapro.2021.05.042.

[5] J. Dąbrowa and M. Danielewski, "State-of-the-art diffusion studies in the high entropy alloys," *Metals (Basel).*, vol. 10, no. 3, 2020, doi: 10.3390/met10030347.

[6] J. P. Oliveira *et al.*, "Gas tungsten arc welding of as-rolled CrMnFeCoNi high entropy alloy," *Mater. Des.*, vol. 189, p. 108505, 2020, doi: 10.1016/j.matdes.2020.108505.

[7] J. Guo *et al.*, "Welding of high entropy alloys-A review," *Entropy*, vol. 21, no. 4, pp. 1–17, 2019, doi: 10.3390/e21040431.

[8] C. Han, Q. Fang, Y. Shi, S. B. Tor, C. K. Chua, and K. Zhou, "Recent Advances on High-Entropy Alloys for 3D Printing," *Adv. Mater.*, vol. 32, no. 26, pp. 1–41, 2020, doi: 10.1002/adma.201903855.

[9] J. G. Lopes and J. P. Oliveira, "A short review on welding and joining of high entropy alloys," *Metals (Basel).*, vol. 10, no. 2, 2020, doi: 10.3390/met10020212.

[10] C. Zhang, J. Zhu, H. Zheng, H. Li, S. Liu, and G. J. Cheng, "A review on microstructures and properties of high entropy alloys manufactured by selective laser melting," *Int. J. Extrem. Manuf.*, vol. 2, no. 3, 2020, doi: 10.1088/2631-7990/ab9ead.

[11] B. Wang *et al.*, "Mechanical Properties and Microstructure of the CoCrFeMnNi High Entropy Alloy Under High Strain Rate Compression," *J. Mater. Eng. Perform.*, vol. 25, no. 7, pp. 2985–2992, 2016, doi: 10.1007/s11665-016-2105-5.

[12] M. Vaidya, K. Guruvidyathri, and B. S. Murty, "Phase formation and thermal stability of CoCrFeNi and CoCrFeMnNi equiatomic high entropy alloys," *J. Alloys Compd.*, vol. 774, pp. 856–864, 2019, doi: 10.1016/j.jallcom.2018.09.342.

[13] Y. K. Kim, M. S. Baek, S. Yang, and K. A. Lee, "In-situ formed oxide enables extraordinary high-cycle fatigue resistance in additively manufactured CoCrFeMnNi high-entropy alloy," *Addit. Manuf.*, vol. 38, no. October 2020, p. 101832, 2021, doi: 10.1016/j.addma.2020.101832.

[14] H. Zhang, Y. Zhao, S. Huang, S. Zhu, F. Wang, and D. Li, "Manufacturing and analysis of high-performance refractory high-entropy alloy via selective laser melting (SLM)," *Materials (Basel).*, vol. 12, no. 5, 2019, doi: 10.3390/ma12050720.

[15] A. Ostovari Moghaddam, N. A. Shaburova, M. N. Samodurova, A. Abdollahzadeh, and E. A. Trofimov, "Additive manufacturing of high entropy alloys: A practical review," *J. Mater. Sci. Technol.*, vol. 77, pp. 131–162, 2021, doi: 10.1016/j.jmst.2020.11.029.

[16] Z. Tang, "Processing, Microstructures, and Mechanical Behavior of High-Entropy Alloys," 2012, [Online]. Available:

https://trace.tennessee.edu/utk_gradthes/1419.
[17] K. B. Small, D. A. Englehart, and T. A. Christman, "Guide to etching specialty alloys," *Adv. Mater. Process.*, vol. 166, no. 2, pp. 32–37, 2008.
[18] S. A. A. Shams, G. Kim, J. W. Won, J. N. Kim, H. S. Kim, and C. S. Lee, "Effect of grain size on the low-cycle fatigue behavior of carbon-containing high-entropy alloys," *Mater. Sci. Eng. A*, vol. 810, p. 140985, Apr. 2021, doi: 10.1016/j.msea.2021.140985.
[19] P. Litwa, E. Hernandez-Nava, D. Guan, R. Goodall, and K. K. Wika, "The additive manufacture processing and machinability of CrMnFeCoNi high entropy alloy," *Mater. Des.*, vol. 198, p. 109380, Jan. 2021, doi: 10.1016/j.matdes.2020.109380.
[20] H. Li, Y. Huang, J. Sun, and Y. Lu, "The relationship between thermo-mechanical history, microstructure and mechanical properties in additively manufactured CoCrFeMnNi high entropy alloy," *J. Mater. Sci. Technol.*, vol. 77, pp. 187–195, Jun. 2021, doi: 10.1016/j.jmst.2020.10.052.
[21] S. A. A. Shams *et al.*, "Low-cycle fatigue properties of CoCrFeMnNi high-entropy alloy compared with its conventional counterparts," *Mater. Sci. Eng. A*, vol. 792, p. 139661, Aug. 2020, doi: 10.1016/j.msea.2020.139661.
[22] B. Wang, M. Sun, B. Li, L. Zhang, and B. Lu, "Anisotropic Response of CoCrFeMnNi High-Entropy Alloy Fabricated by Selective Laser Melting," *Materials (Basel).*, vol. 13, no. 24, p. 5687, Dec. 2020, doi: 10.3390/ma13245687.
[23] J. Čech, P. Haušild, M. Karlík, J. Čapek, and F. Průša, "Indentation Size Effect in CoCrFeMnNi HEA Prepared by Various Techniques," *Materials (Basel).*, vol. 14, no. 23, p. 7246, Nov. 2021, doi: 10.3390/ma14237246.
[24] J. P. Oliveira *et al.*, "Improving the ductility in laser welded joints of CoCrFeMnNi high entropy alloy to 316 stainless steel," *Mater. Des.*, vol. 219, p. 110717, Jul. 2022, doi: 10.1016/j.matdes.2022.110717.
[25] J. W. Pegues, M. A. Melia, R. Puckett, S. R. Whetten, N. Argibay, and A. B. Kustas, "Exploring additive manufacturing as a high-throughput screening tool for multiphase high entropy alloys," *Addit. Manuf.*, vol. 37, p. 101598, Jan. 2021, doi: 10.1016/j.addma.2020.101598.
[26] J. P. Oliveira *et al.*, "Dissimilar laser welding of a CoCrFeMnNi high entropy alloy to 316 stainless steel," *Scr. Mater.*, vol. 206, p. 114219, Jan. 2022, doi: 10.1016/j.scriptamat.2021.114219.
[27] H. F. Brinson and L. C. Brinson, "Stress and Strain Analysis and Measurement," in *Polymer Engineering Science and Viscoelasticity*, Boston, MA: Springer US, 2015, pp. 15–55.
[28] O. P. Choudhary and P. Ka, "Scanning Electron Microscope: Advantages and Disadvantages in Imaging Components," *Int. J. Curr. Microbiol. Appl. Sci.*, vol. 6, no. 5, pp. 1877–1882, May 2017, doi: 10.20546/ijcmas.2017.605.207.

6

APPENDIX

A. Polishing machine and papers

A1. Polishing machine

A2. Abrasive papers

B. HEA 1 microstructure

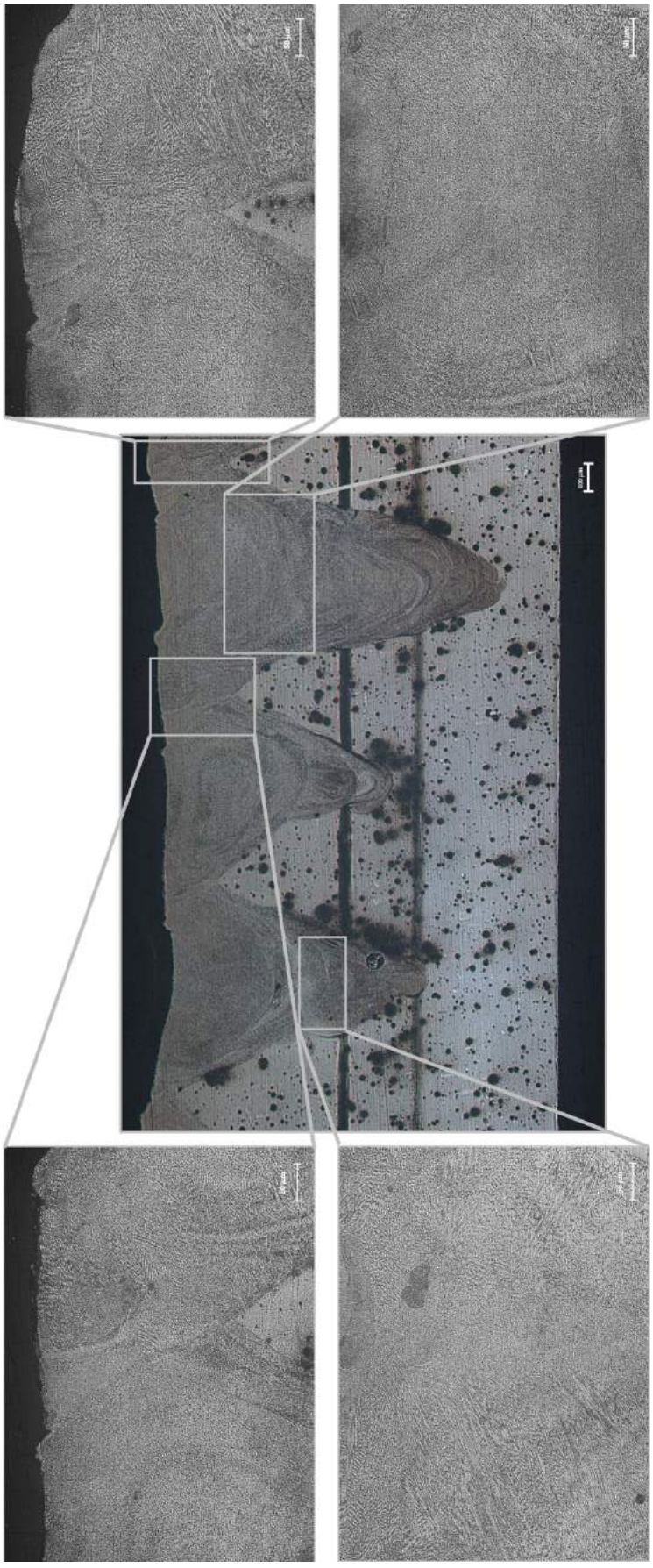

C. HEA 2 microstructure

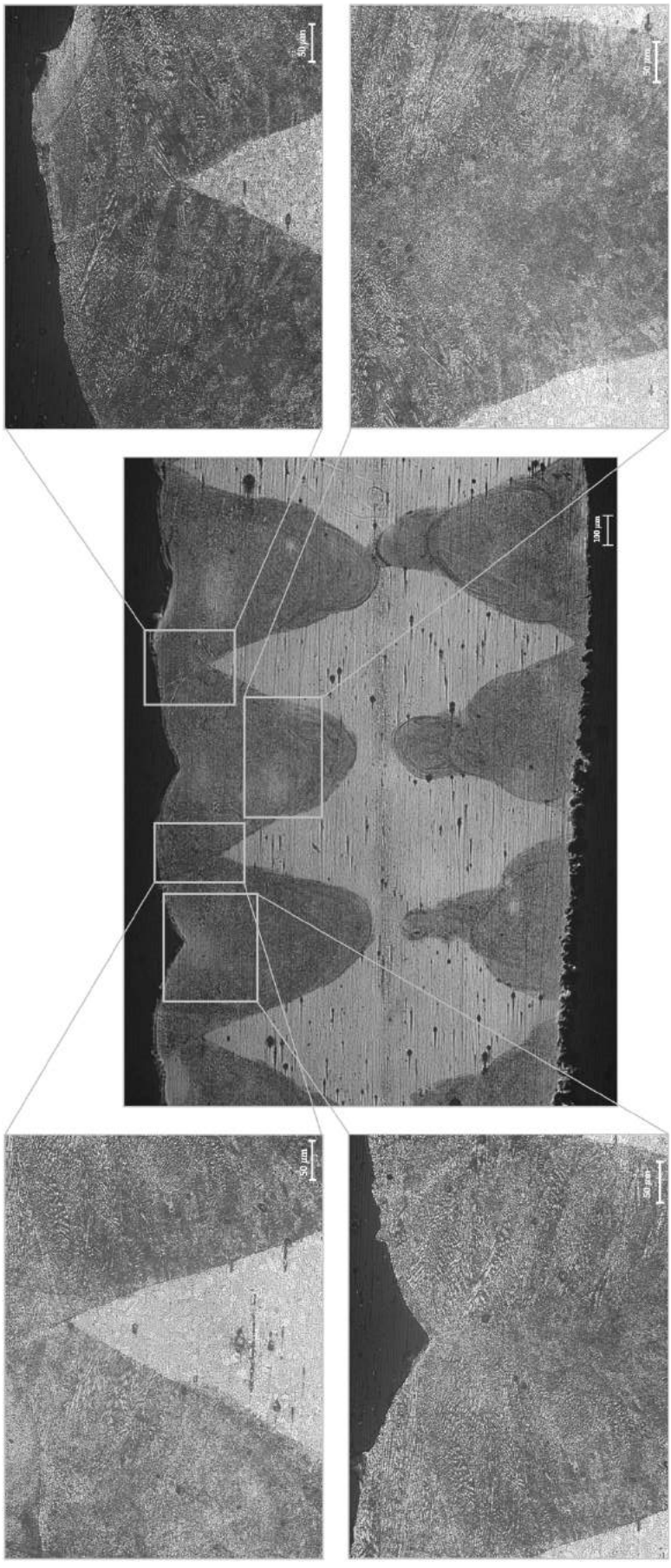

D. EBSD mapping on HEA 1